NANO LETTERS

Letter

pubs.acs.org/NanoLett

Computational Synthesis of MoS_2 Layers by Reactive Molecular Dynamics Simulations: Initial Sulfidation of MoO_3 Surfaces

Sungwook Hong,*[,†] Aravind Krishnamoorthy,[†] Pankaj Rajak,[†] Subodh Tiwari,[†] Masaaki Misawa,[‡] Fuyuki Shimojo,[‡] Rajiv K. Kalia,[†] Aiichiro Nakano,[†] and Priya Vashishta[†]

[†]Collaboratory for Advanced Computing and Simulations, Department of Physics & Astronomy, Department of Computer Science, Department of Chemical Engineering & Materials Science, and Department of Biological Sciences, University of Southern California, Los Angeles, California 90089-0242, United States

[‡]Department of Physics, Kumamoto University, Kumamoto 860-8555, Japan

Supporting Information

ABSTRACT: Transition metal dichalcogenides (TMDC) like MoS_2 are promising candidates for next-generation electric and optoelectronic devices. These TMDC monolayers are typically synthesized by chemical vapor deposition (CVD). However, despite significant amount of empirical work on this CVD growth of monolayered crystals, neither experiment nor theory has been able to decipher mechanisms of selection rules for different growth scenarios, or make predictions of optimized environmental parameters and growth factors. Here, we present an atomic-scale mechanistic analysis of the initial sulfidation process on MoO_3 surfaces using first-principles-informed ReaxFF reactive molecular dynamics (RMD) simulations. We identify a three-step reaction process associated with synthesis of the MoS_2 samples from MoO_3 and S_2 precursors: O_2 evolution and self-reduction of the MoO_3 surface; SO/SO_2 formation and S_2-assisted reduction; and sulfidation of the reduced surface and Mo−S bond formation. These atomic processes occurring during early stage MoS_2 synthesis, which are consistent with experimental observations and existing theoretical literature, provide valuable input for guided rational synthesis of MoS_2 and other TMDC crystals by the CVD process.

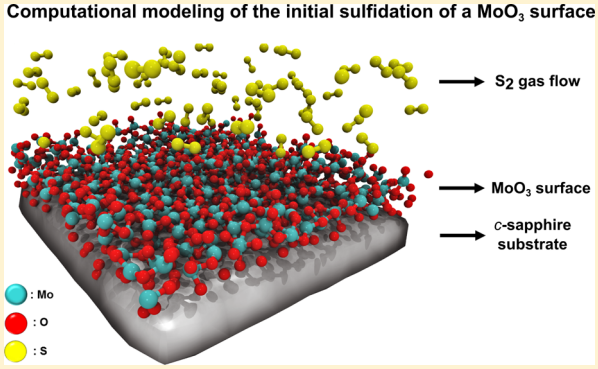

KEYWORDS: *ReaxFF, molecular dynamics simulations, MoO_3 surface, sulfidation, MoS_2, synthesis*

Two-dimensional and layered materials have unique electric and optoelectronic characteristics, distinct from their bulk phases due to the existence of relatively weak interlayer interactions and two-dimensional quantum confinement.[1−3] Graphene was the first to be considered a real two-dimensional material,[6] and it has been extensively studied for nanoscale applications.[4,5] Two-dimensional semiconducting crystals like MoS_2 monolayer are promising candidates for next-generation electronic devices (e.g., ultrathin channel materials) primarily due to (a) the high abundance of molybdenite and the associated low cost, (b) greater carrier mobility than conventional Si-based devices, and (c) nonzero bandgaps, unlike graphene.[6−8] In addition, MoS_2 monolayer can be applied to flexible substrates because of its exceptional mechanical properties[9−12] and can provide active edge sites for the hydrogen evolution reaction.[13] MoS_2 samples for bench-scale devices and experiments are typically synthesized via mechanical exfoliation or chemical vapor deposition (CVD).[14−16] Of these two methods, CVD is the only method that can be scaled up for mass production of monolayered crystals required into consumer applications. While several previous studies have demonstrated the growth of MoS_2 layers from different precursors and have provided qualitative information about reaction pathways leading to crystal growth,[17−23] deciphering selection rules for different growth scenarios to make predictions of optimized environmental parameters and growth factors has remained unclear. This is primarily due to a lack of understanding of mechanistic processes by which the CVD growth of MoS_2 monolayer is achieved. Computational modeling, particularly reactive molecular dynamics (RMD) simulations, can provide useful insights into interfaces[24] and surface−gas interactions[25] on model systems down to atomic length scales. In this work, we perform RMD simulations for computational synthesis of MoS_2 structures using MoO_3 surfaces and gaseous S_2. Our goal is to identify the atomic-level mechanism for the growth of MoS_2 phases by the sulfidation of MoO_3 crystals. The subsequent sections describe the computational methodology for RMD simulations followed by a discussion of the observed mechanism for the reaction between MoO_3 and S_2 to form MoS_2.

Received: April 24, 2017
Revised: June 29, 2017
Published: July 3, 2017

DOI: 10.1021/acs.nanolett.7b01727
Nano Lett. 2017, 17, 4866−4872

Empirical reactive methods such as the COMB[26,27] and ReaxFF[28] potentials allow for large-scale RMD simulations with a well-documented variable-charge scheme.[29] In this study, ReaxFF reactive force field parameters for Mo/O and Mo/S interactions were extracted from Chenoweth et al.[30] and Ostadhossein et al.,[31] respectively, and then reoptimized to more accurately describe reaction events between the MoO_3 surface and S_2 molecules. In addition, ReaxFF reactive force field parameters for S/O interactions, successfully applied to a previous study,[32] were taken to capture CVD processes; the Supporting Information includes quantum mechanical (QM) data used for a ReaxFF force field training set and results of the force field reoptimization. Detailed information on ReaxFF and its applications is available in review papers.[33,34] ReaxFF force field parameters were then coupled with RMD simulations. Small integration time steps of 0.25−0.30 fs were used with the NVT ensemble to properly describe chemical reactions. To control system temperatures, the Nose−Hoover thermostat[35,36] with a temperature damping constant of 25.0 fs was applied to the whole system including gas and surface models. We simulated a MoO_3 layer supported on an Al_2O_3 substrate, exposed to S_2 atmosphere, following a recent experimental setup (Figure 1a).[21] All simulations were done on a simulation

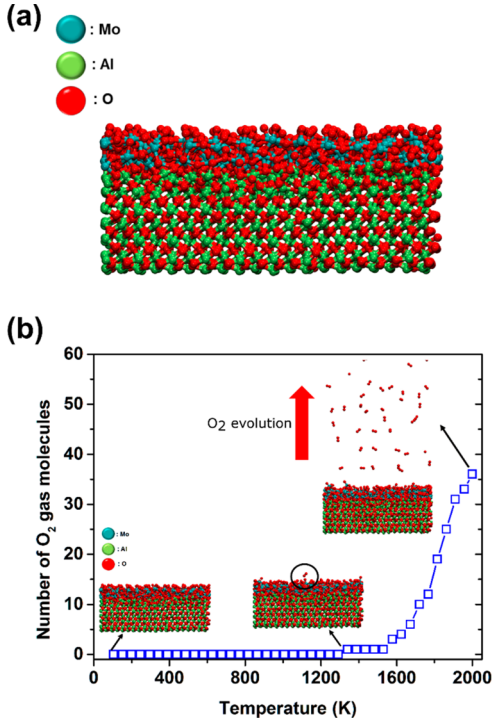

Figure 1. (a) Initial configuration of the MoO_3/Al_2O_3 surface. The surface was annealed at 500 K for 125 ps and cooled down to 100 K for 25 ps. (b) Number of O_2 gas molecules evolved from the MoO_3 surface as a function of instantaneous temperature, and corresponding RMD snapshots at 0, 1300, and 2000 K. The black circle in the snapshot at 1300 K represents the onset of O_2 evolution.

cell of lateral dimensions (47.09 Å × 45.57 Å) containing one monolayer of MoO_3 (~6 Å thick) supported on an Al_2O_3 (0001) surface (~15 Å thick); the Al_2O_3 surface serves as a substrate, while MoO_3 surface provides Mo sources on the substrate for the growth of MoS_2 structures. This combined surface structure, consisting of the α-MoO_3(001) surface (1152 atoms) supported by the α-Al_2O_3(0001) surface (3375 atoms) was relaxed using a conjugate gradient method, followed by thermal equilibration at 500 K for 125 ps, and then cooled down to 100 K for 25 ps. This simulation schedule leads to a model of a MoO_3 predeposited on Al_2O_3, consistent with experimental studies.[21,37] For CVD synthesis of atomically thin MoS_2 layers, both MoO_3 and S powders are generally employed as initial reactants. However, the experimental studies in refs 21 and 37 indicated that wafer-scale MoS_2 layers with great uniformity can be effectively synthesized by using a predeposited MoO_3 surface, instead of vaporized MoO_3 power, as a starting material. Thus, we chose to use the predeposited MoO_3 surface on the Al_2O_3 surface for RMD simulations. Although our simulation model is dissimilar to the one from experimental methods typically using MoO_3 and sulfur powders,[38,39] our study still provides key reaction events for the sulfidation of MoO_3 that eventually enables us to understand the conventional CVD process of MoS_2 layers. Furthermore, as discussed above, our simulation model is consistent with the experimental setup that used the MoO_3 predeposited on Al_2O_3 substrate, thus providing a better understanding of reaction mechanisms for the sulfidation of the MoO_3 surface using S_2 gas molecules. For CVD simulations, we placed the surface model along with gaseous S_2 in vacuum layers of 100 Å. In doing so, CVD processes can be reproduced by our RMD simulations using chemical reactions of the MoO_3 surface and S_2 gas molecules. In light of relatively high temperatures during our ReaxFF-RMD simulations (up to 2300 K), compared to experimental CVD conditions (~1200 K),[40,41] a one-body spring force was added to each atom in the α-Al_2O_3(0001) surface to prevent interdiffusion of the Al_2O_3 and MoO_3. This ensures that the α-Al_2O_3(0001) surface behaves as a nonreactive surface for our RMD simulations. In addition, a periodic boundary condition was used in the x- and y-directions, while a wall boundary condition was applied to the z-direction to prevent the diffusion of gas-phase atoms across the boundary and potentially reacting with the bottom of the α-Al_2O_3 surface.

Our RMD simulations identify a three-step reaction pathway for the synthesis of MoS_2 crystals by the sulfidation (by S_2 gas) of MoO_3 monolayers: 1. O_2 evolution and self-reduction of the MoO_3 surface; 2. SO/SO_2 formation and S_2-assisted reduction; 3. Sulfidation of the reduced surface and Mo−S bond formation. This section reports the three reaction processes stepwise.

O_2 Evolution and Self-Reduction of the MoO_3 Surface. To elucidate the surface chemistry of MoO_3(001) at high temperatures, the MoO_3/Al_2O_3 surface (see Figure 1a) was heated from 100 to 2000 K at a heating rate of 0.002 K/fs. Figure 1b shows the number of O_2 gas molecules evolved from the MoO_3 surface as a function of the instantaneous temperature of the system, described by the ReaxFF-RMD simulations. O_2 evolution begins at approximately 1300 K, which lies above the reported melting point and below the sublimation point of the MoO_3 crystal,[42] suggesting that O_2 evolution occurs from a disordered, noncrystalline MoO_3 structure. Our RMD simulations show that O_2 molecules are predominantly generated due to the cleavage of the terminal Mo═O_t double bonds or the weaker, asymmetric bridging Mo−O−Mo bonds in-plane. Basically, our ReaxFF description has shown its ability to reasonably describe bulk properties and thermal stabilities of α-phase MoO_3 crystal structure, consistent with experimental and density functional theory (DFT) literature (see Supporting Information for details of ReaxFF

DOI: 10.1021/acs.nanolett.7b01727
Nano Lett. 2017, 17, 4866−4872

reactive force field validation). In addition, based on previous experimental observations,[43] the O-termination site in crystalline MoO_3 is known to be the most reactive entity, thus preferably reacting with each other and leading to O_2 evolution. Namely, the mechanisms for O_2 evolution and MoO_3 reduction by our RMD simulations are in excellent agreement with experimental observations in ref 43 as follows:

$$2 - Mo^{n}{=}O_t \rightarrow 2 - Mo^{(n-1)+} + O_2(g)\uparrow \quad (1)$$

$$-Mo^{n+}(=O_t)_2 \rightarrow -Mo^{(n-2)+} + O_2(g)\uparrow \quad (2)$$

To evaluate the unit processes involved in O_2 evolution from the MoO_3 surface in more detail and to quantify the effect of structural disorder on O_2 evolution, we performed ReaxFF-nudged elastic band (ReaxFF-NEB) calculations to evaluate activation barriers. Specifically, we compared reaction paths calculated for identical O_2 evolution reactions on MoO_3 surfaces at low and high temperatures. Low-temperature surface structures correspond to the 0 K ground state structure of the $MoO_3(001)$ surface, while high-temperature structures are constructed from snapshots of the RMD simulations at an instantaneous temperature of 2000 K. Figure 2 demonstrates

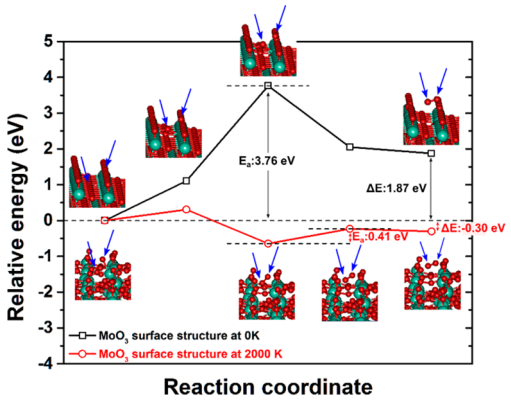

Figure 2. ReaxFF-NEB calculations of reaction paths for the O_2 evolution at the MoO_3 surface structure 0 K (black hollow square) and 2000 K (red hollow circle). Blue arrows represent O atoms participating in the O_2 evolution; one originates from the O-termination site and the other one from the Mo−O−Mo bridge). Note that the distorted MoO_3 structure (2000 K) lowers the largest reaction barrier to 0.41 eV and changes the reaction to exothermic (−0.30 eV), making the O_2 evolution favorable thermodynamically and kinetically (cyan balls and sticks, Mo atoms; red balls and sticks, O atoms).

that O_2 evolution from the distorted high-temperature surface is moderately exothermic (ΔE = −0.30 eV) and has an activation barrier of 0.41 eV, in contrast to the crystalline ground-state surface, which shows a high endothermicity and a high activation barrier (ΔE = 1.87 eV, E_a = 3.76 eV) that renders O_2 evolution kinetically and energetically unfavorable at low temperatures. These results suggest that high-temperature-induced structural distortion is necessary for O_2 evolution, which leads to the generation of unsaturated Mo sites on the MoO_3 surface for subsequent sulfidation.

To investigate the kinetics of the thermal reduction process on MoO_3 surfaces, we held the MoO_3/Al_2O_3 surface described previously at a high temperature of 2000 K for 775 ps, and followed the O_2 evolution process as a function of time. As shown in Figure 3a, the number of O_2 gas molecules displays

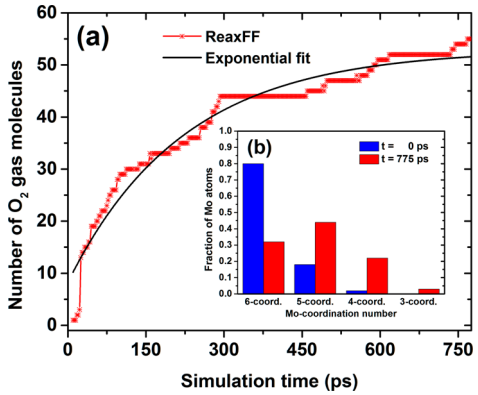

Figure 3. ReaxFF-RMD simulations of O_2 evolution from a MoO_3 surface held at 2000 K. (a) Number of O_2 gas molecules evolved as a function of time at 2000 K. (b) Histogram of coordination number of Mo atoms in the MoO_3 surface in the low-temperature, stoichiometric crystal (blue) compared with the reduced surface after 750 ps of reduction at 2000 K. At 100 K (0 ps), most Mo-coordination consisted of 6-coordination (a small portion of 5- and 4-coordination was also observed because the initial MoO_3/Al_2O_3 surface was thermally equilibrated at 500 K and thus the atoms' positions were rearranged). At 2000 K (775 ps), the 6-coordination was reduced to 5-, 4-, and 3-coordiation, indicating that the number of unsaturated Mo atoms increased.

monotonic exponential kinetics, leading to a partially reduced $MoO_{2.6}$ surface at 775 ps. Figure 3b shows the histogram for coordination number for Mo atoms in the MoO_3 surface at t = 0 and t = 775 ps. O_2 evolution during the high-temperature annealing process causes the 6-fold coordinated Mo atoms at low temperature to become undersaturated 5-fold, 4-fold, and 3-fold coordinated Mo atoms (i.e., self-reduction), which act as reaction sites for subsequent sulfidation reactions.

SO/SO_2 Formation and S_2-Assisted Reduction. To investigate whether the undersaturated Mo atoms activate toward subsequent sulfidation, we performed first-principles QM calculations based on DFT. Section 2.3 in the Supporting Information shows DFT-based nudged elastic band (DFT-NEB) calculations of S_2 adsorption on a $MoO_3(010)$ with an O-vacancy. The DFT-NEB calculations were also used to validate the ReaxFF force field. The ReaxFF-NEB results on reaction barrier (0.22 eV) and energy (−1.11 eV) for the S_2 adsorption on the MoO_3 (010) with an O-vacancy quantitatively agree with our DFT-NEB calculations, thus validating the ReaxFF force field for this key reaction. The relatively low barrier and high exothermicity suggest that the reduced MoO_x surface is necessary for making sulfidation reactions preferable.

Based on this observation, the reduced $MoO_{2.6}/Al_2O_3$ surface from the previous section was then placed in contact with an atmosphere of 400 S_2 gas molecules in the simulation cell (corresponding to a density of S_2 gas: 0.23 g/cm^3) to perform ReaxFF-RMD simulations of the sulfidation process. Figure 4a,b shows the initial and final snapshots of the ReaxFF-RMD simulations at 2300 K, respectively. After 1.2 ns, it is worth noting that S_2 gas molecules reacted with the $MoO_{2.6}$ surface, leading to the formation of SO and SO_2 gas products (inset in Figure 4b). Based on trajectories of the ReaxFF-RMD simulations, the primary reaction mechanisms for SO and SO_2 formation can be summarized as follows:

DOI: 10.1021/acs.nanolett.7b01727
Nano Lett. 2017, 17, 4866−4872

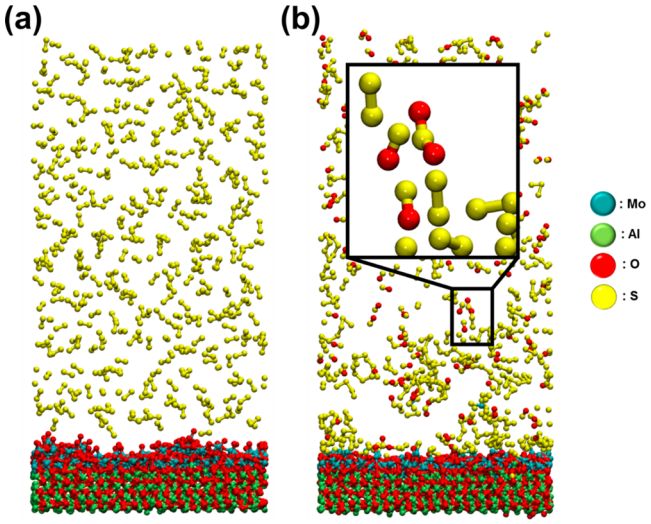

Figure 4. Snapshots of sulfidation at the $MoO_{2.6}/Al_2O_3$ surface described by the ReaxFF-RMD simulations (a) at 0 ns and (b) at 1.2 ns. Note that 97% of gas products consists of SO molecules (3% for SO_2 molecules).

$$-\mathrm{Mo} = \mathrm{S_2}^* + -\mathrm{Mo}{=}\mathrm{O_t}^* \rightarrow -\mathrm{Mo}{-}\mathrm{S}^* + -\mathrm{Mo}{=}^* + \mathrm{SO(g)}\uparrow \quad (3)$$

$$-\mathrm{Mo}{=}\mathrm{O_t}^* + \mathrm{SO(g)} \rightarrow -\mathrm{Mo}{=}^* + \mathrm{SO_2(g)}\uparrow \quad (4)$$

where an asterisk represents a surface species. S_2 molecules were found to participate both in the further reduction of the $MoO_{2.6}$ structure as well as the sulfidation of the reduced surface, thus validating mechanisms hypothesized in a previous experimental study.[44] In addition, the reaction mechanisms described by our RMD simulations were qualitatively consistent with a previous study[22] reporting that MoO_3 reactants are reduced by sulfur gas to form oxysulfide species (MoO_xS_y), resulting in the formation of SO_x products. Consequently, the $MoO_{2.6}$ surface transformed to a $MoO_{1.99}S_{0.24}$ surface structure (Table 1). To support the robustness of the ReaxFF description for describing the surface reactions above, we constructed ground-state structures containing S_2/MoO_3 surface interactions: S_2 dissociation on the MoO_3 surface and SO_2 desorption from the MoO_3 surface. Then, DFT- and ReaxFF-NEB calculations were conducted to investigate reaction energies and barriers (see Supporting Information for details of DFT-NEB calculations). As shown in Figure 5a,b, the reaction barriers and energies of the above cases, as proposed by the ReaxFF-NEB calculations, were quantitatively consistent with the DFT-NEB calculations, thus validating the ability of the ReaxFF description to properly capture reaction events between S_2 gas and the MoO_3 surface. The ReaxFF-NEB results indicate that S_2 dissociation on the MoO_3 surface is somewhat endothermic (reaction energy of 0.15 eV) with a mild barrier

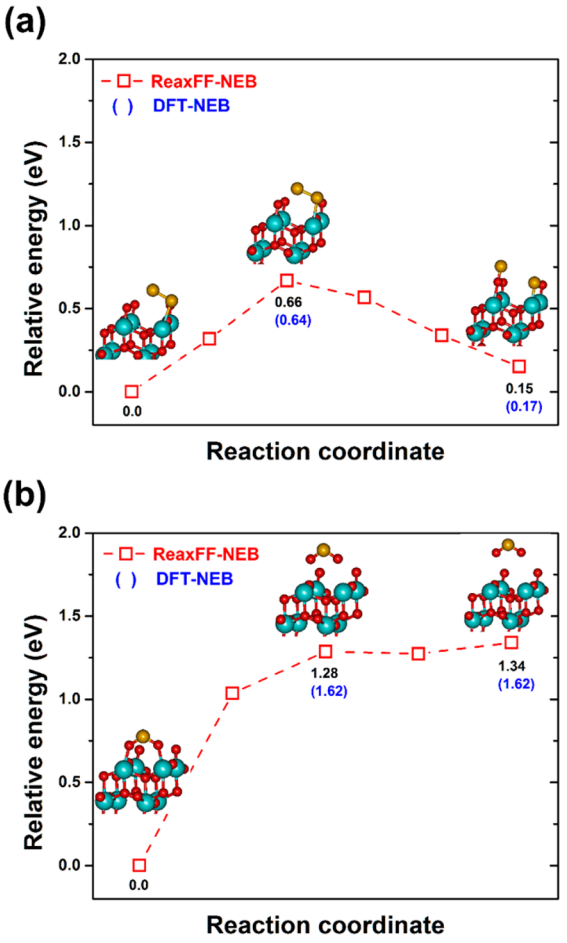

Figure 5. ReaxFF-NEB calculations of reaction paths for (a) S_2 dissociation from the O-vacancy site on the MoO_3 surface and (b) SO_2 desorption from the O-vacancy site on the MoO_3 surface. The initial MoO_3 surface structure was taken from the ground state structure. Reaction barriers and energies from the DFT-NEB calculations (blue parentheses) indicate that the ReaxFF can correctly capture reaction events associated with S_2/MoO_3 interactions (cyan, Mo atoms; red, O atoms; yellow, S atoms).

Table 1. Surface Structures of MoO_xS_y Obtained by the Stepwise ReaxFF-RMD Simulations[a]

simulation step	temperature (K)	accumulated time (ns)	number of atoms of each species on the reacting surface			surface composition
			Mo	O	S	
initial	0	0.000	288	864	0	MoO_3
annealing	2000	0.775	288	748	0	$MoO_{2.60}$
sulfidation	2300	1.975	286	571	70	$MoO_{1.99}S_{0.24}$
sulfidation	2300	3.175	286	539	99	$MoO_{1.88}S_{0.35}$
sulfidation	2300	7.975	263	447	147	$MoO_{1.70}S_{0.56}$
cooling	300	8.125	263	447	147	$MoO_{1.70}S_{0.56}$

[a]An annealing process was conducted for the first 0.775 ns, followed by a sulfidation process for a further 7.200 ns. Subsequently, the surface structure was cooled down to 300 K for 0.150 ns. During the sulfidation process, all gas products were removed, and intact S_2 gas molecules were added every 1.2 ns. Note that the initial MoO_3 surface structure converted to a $MoO_{1.70}S_{0.56}$ surface structure at the accumulated time of 8.125 ns.

DOI: 10.1021/acs.nanolett.7b01727
Nano Lett. 2017, 17, 4866−4872

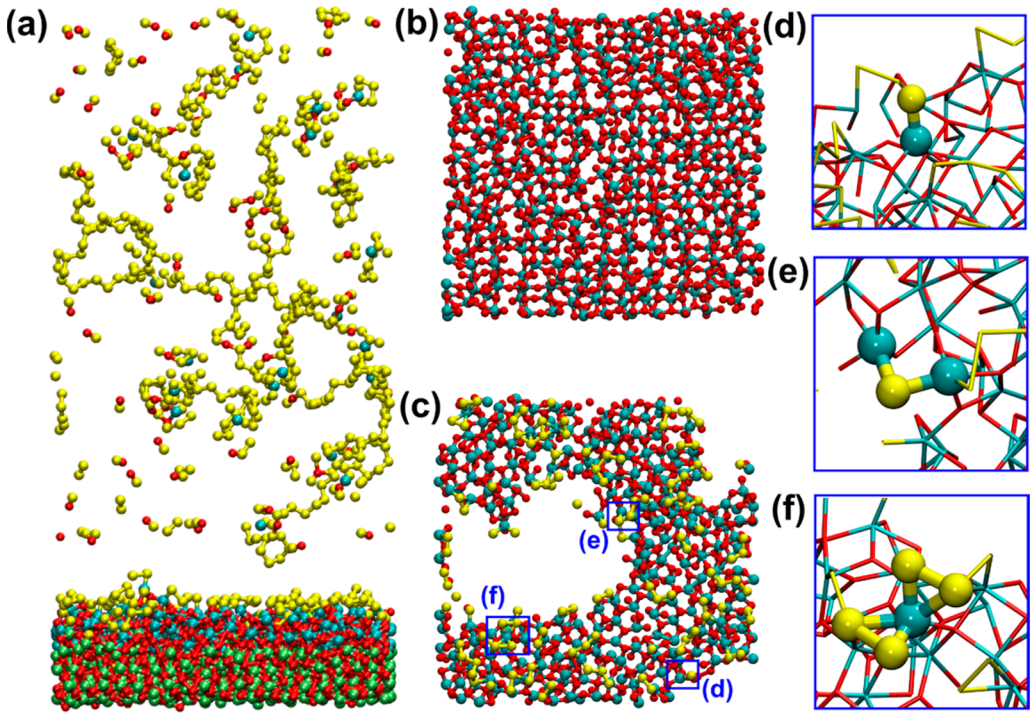

Figure 6. (a) Snapshot of the RMD simulation cell at 8.125 ns. (b,c) Top views of the MoO_3 (0 ns) and $MoO_{1.70}S_{0.56}$ surface (8.125 ns) structures, respectively; Al and O atoms in the Al_2O_3 layer are hidden for clarity. Significant voids were observed on the $MoO_{1.70}S_{0.56}$ surface due to Mo atoms' redistribution during the reduction and sulfidation processes. (d–f) Close-ups of Mo–S termination, Mo–S–Mo bridge, and $Mo(S_2)_2$ edge structures, respectively, as highlighted in (c). Note that three structures describe a small portion of MoS_2 structures, which can be further grown to form MoS_2-like crystals (cyan balls and sticks, Mo; lime balls and sticks, Al; red balls and sticks, O; yellow balls and sticks, S).

(0.66 eV), and that the SO_2 desorption from the MoO_3 surface is a much more unfavorable reaction, as the total energy increased to 1.34 eV. As such, one can expect that surface reactions associated with SO_2 formation will be energetically unfavorable compared with SO formation. These analyses can aid in explaining the observation of a relatively large number of SO gas products (97% of gas products), compared to that of the SO_2 gas products (3% of gas products) during the ReaxFF-RMD simulations at 2300 K. Therefore, we suggest that further reduction and sulfidation of the $MoO_{2.6}$ surface can be achieved by two reaction processes at high temperatures: primarily SO formation, followed by SO_2 formation.

Sulfidation of the Reduced Surface and Extensive Mo–S Bond Formation. To further observe Mo–S bonds formation, we extended our ReaxFF-RMD simulations for the sulfidation at the partially reduced and partially sulfurized $MoO_{1.99}S_{0.24}$ surface from the previous section for a further 6.0 ns, after which the final surface structure was cooled down to 100 K for additional 0.15 ns. In order to simulate the flow of the gas phase over the reacting surface in CVD growth conditions, all gas molecules in the simulation cell were purged every 1.2 ns and replaced with pure S_2 molecules. Figure 6a shows a final snapshot of the surface structure from the ReaxFF-RMD simulations. As shown in Table 1, the final structure at an accumulated reaction time of 8.125 ns corresponds to a $MoO_{1.70}S_{0.56}$ surface, indicating that further O atoms in the MoO_xS_y surface were substituted by S atoms and additional S_2 molecules chemisorbed on the MoO_xS_y surface. It is interesting to note that, during the ReaxFF-RMD simulations of the sulfidation process, significant voids on the Al_2O_3 substrate were generated as the initial MoO_3 surface structure converted to the $MoO_{1.70}S_{0.56}$ surface structure, resulting in the Mo atoms' migration and reorganization on the Al_2O_3 substrate (see Figure 6b,c). These results are consistent with the early stage of the sulfidation process at the MoO_3 predeposited sapphire substrate by Taheri et al.[37] Their experimental study reported that the growth of MoS_2 monolayer involved not only S substitutions on the MoO_3 surface but also Mo atoms' redistribution, and thus, voids were observed when forming discrete MoS_2 triangles. In addition, Mo/S configurations on the final $MoO_{1.70}S_{0.56}$ surface structure qualitatively matched with a portion of monolayered MoS_2 crystal structure; the Mo/S structures from the ReaxFF-RMD simulations exhibit a proportion of S-termination, Mo–S–Mo bridge, and MoS_2 edge structures, as shown in Figure 6d–f, respectively. Based on our observations, it is expected that when exposing to more S_2 gas flow, surface structures like stoichiometric MoS_2 crystals can be synthesized. While further growth and follow-up crystallization of MoS_2 monolayers will be studied in the future, the present ReaxFF-RMD simulations confirm that the initial sulfidation process of the MoO_3 surface is achieved by three reaction steps.

In summary, we investigated the computational synthesis of MoS_2 layers from deposited MoO_3 and gaseous S_2 precursors using ReaxFF-RMD simulations with reoptimized force field parameters for Mo/O/S. The ReaxFF-RMD simulations demonstrated that a portion of the MoS_2 species can be synthesized via a three-step reaction mechanism: 1. O_2 evolution and self-reduction of the MoO_3 surface, 2. SO/SO_2 formation and S_2-assisted reduction, and 3. Sulfidation of the reduced surface and Mo–S bond formation. The atomic resolution of the RMD simulations allows us to elucidate

DOI: 10.1021/acs.nanolett.7b01727
Nano Lett. 2017, 17, 4866–4872

important details about the synthesis process, like the requirement of a disordered surface structure, and the dual role of S_2 molecules as reducing and sulfidizing agents. In that sense, our approach opens a promising direction to explore complex reaction processes for synthesis of MoS_2 monolayers, and other two-dimensional materials.

■ ASSOCIATED CONTENT

Supporting Information

The Supporting Information is available free of charge on the ACS Publications website at DOI: 10.1021/acs.nanolett.7b01727.

ReaxFF reactive force field reoptimization and validation for Mo/O/S interactions (PDF)

■ AUTHOR INFORMATION

Corresponding Author

*E-mail: sungwooh@usc.edu.

ORCID

Sungwook Hong: 0000-0003-3569-7701

Aravind Krishnamoorthy: 0000-0001-6778-2471

Author Contributions

S.H. and A.K. contributed equally to this work.

Notes

The authors declare no competing financial interest.

■ ACKNOWLEDGMENTS

This work was supported as part of the Computational Materials Sciences Program funded by the U.S. Department of Energy, Office of Science, Basic Energy Sciences, under Award Number DE-SC00014607. The simulations were performed at the Argonne Leadership Computing Facility under the DOE INCITE program and at the Center for High Performance Computing of the University of Southern California. S.H. thanks Prof. Adri van Duin for providing valuable information on initial ReaxFF force field parameters for Mo/O/S elements.

■ REFERENCES

(1) Gupta, A.; Sakthivel, T.; Seal, S. *Prog. Mater. Sci.* **2015**, *73*, 44−126.

(2) Venkata Subbaiah, Y.; Saji, K.; Tiwari, A. *Adv. Funct. Mater.* **2016**, *26*, 2046−2069.

(3) Zhang, Y.; Tan, Y.-W.; Stormer, H. L.; Kim, P. *Nature* **2005**, *438*, 201−204.

(4) Qin, Z.; Taylor, M.; Hwang, M.; Bertoldi, K.; Buehler, M. J. *Nano Lett.* **2014**, *14*, 6520−6525.

(5) Shahil, K. M.; Balandin, A. A. *Solid State Commun.* **2012**, *152*, 1331−1340.

(6) Li, X.; Zhu, H. *J. Materiomics* **2015**, *1*, 33−44.

(7) Mak, K. F.; Lee, C.; Hone, J.; Shan, J.; Heinz, T. F. *Phys. Rev. Lett.* **2010**, *105*, 136805.

(8) Nair, R. R.; Ren, W.; Jalil, R.; Riaz, I.; Kravets, V. G.; Britnell, L.; Blake, P.; Schedin, F.; Mayorov, A. S.; Yuan, S. *Small* **2010**, *6*, 2773−2773.

(9) Kaplan, D.; Gong, Y.; Mills, K.; Swaminathan, V.; Ajayan, P.; Shirodkar, S.; Kaxiras, E. *2D Mater.* **2016**, *3*, 015005.

(10) Wang, Q. H.; Kalantar-Zadeh, K.; Kis, A.; Coleman, J. N.; Strano, M. S. *Nat. Nanotechnol.* **2012**, *7*, 699−712.

(11) Lee, G.-H.; Yu, Y.-J.; Cui, X.; Petrone, N.; Lee, C.-H.; Choi, M. S.; Lee, D.-Y.; Lee, C.; Yoo, W. J.; Watanabe, K. *ACS Nano* **2013**, *7*, 7931−7936.

(12) Pu, J.; Yomogida, Y.; Liu, K.-K.; Li, L.-J.; Iwasa, Y.; Takenobu, T. *Nano Lett.* **2012**, *12*, 4013−4017.

(13) Li, H.; Tsai, C.; Koh, A. L.; Cai, L.; Contryman, A. W.; Fragapane, A. H.; Zhao, J.; Han, H. S.; Manoharan, H. C.; Abild-Pedersen, F.; Nørskov, J. K.; Zheng, X. *Nat. Mater.* **2015**, *15*, 48.

(14) Zhang, W.; Zhang, P.; Su, Z.; Wei, G. *Nanoscale* **2015**, *7*, 18364−18378.

(15) Lv, Z.; Mahmood, N.; Tahir, M.; Pan, L.; Zhang, X.; Zou, J.-J. *Nanoscale* **2016**, *8*, 18250−18269.

(16) Yu, J.; Li, J.; Zhang, W.; Chang, H. *Chem. Sci.* **2015**, *6*, 6705−6716.

(17) Ganatra, R.; Zhang, Q. *ACS Nano* **2014**, *8*, 4074−4099.

(18) Lee, Y. H.; Zhang, X. Q.; Zhang, W.; Chang, M. T.; Lin, C. T.; Chang, K. D.; Yu, Y. C.; Wang, J. T. W.; Chang, C. S.; Li, L. J. *Adv. Mater.* **2012**, *24*, 2320−2325.

(19) van der Zande, A. M.; Huang, P. Y.; Chenet, D. A.; Berkelbach, T. C.; You, Y.; Lee, G.-H.; Heinz, T. F.; Reichman, D. R.; Muller, D. A.; Hone, J. C. *Nat. Mater.* **2013**, *12*, 554−561.

(20) Liu, Z.; Amani, M.; Najmaei, S.; Xu, Q.; Zou, X.; Zhou, W.; Yu, T.; Qiu, C.; Birdwell, A. G.; Crowne, F. J. *Nat. Commun.* **2014**, *5*, 5246.

(21) Lin, Y.-C.; Zhang, W.; Huang, J.-K.; Liu, K.-K.; Lee, Y.-H.; Liang, C.-T.; Chu, C.-W.; Li, L.-J. *Nanoscale* **2012**, *4*, 6637−6641.

(22) Jeon, J.; Lee, J.; Yoo, G.; Park, J.-H.; Yeom, G. Y.; Jang, Y. H.; Lee, S. *Nanoscale* **2016**, *8*, 16995−17003.

(23) Zhan, Y.; Liu, Z.; Najmaei, S.; Ajayan, P. M.; Lou, J. *Small* **2012**, *8*, 966−971.

(24) Mo, Y.; Turner, K. T.; Szlufarska, I. *Nature* **2009**, *457*, 1116−1119.

(25) Mueller, J. E.; van Duin, A. C. T.; Goddard, W. A., III *J. Phys. Chem. C* **2010**, *114*, 4939−4949.

(26) Liang, T.; Devine, B.; Phillpot, S. R.; Sinnott, S. B. *J. Phys. Chem. A* **2012**, *116*, 7976−7991.

(27) Shan, T.-R.; Devine, B. D.; Hawkins, J. M.; Asthagiri, A.; Phillpot, S. R.; Sinnott, S. B. *Phys. Rev. B: Condens. Matter Mater. Phys.* **2010**, *82*, 235302.

(28) van Duin, A. C. T.; Dasgupta, S.; Lorant, F.; Goddard, W. A. *J. Phys. Chem. A* **2001**, *105*, 9396−9409.

(29) Liang, T.; Shin, Y. K.; Cheng, Y.-T.; Yilmaz, D. E.; Vishnu, K. G.; Verners, O.; Zou, C.; Phillpot, S. R.; Sinnott, S. B.; van Duin, A. C. T. *Annu. Rev. Mater. Res.* **2013**, *43*, 109−129.

(30) Chenoweth, K.; van Duin, A. C. T.; Goddard, W. A. *Angew. Chem., Int. Ed.* **2009**, *48*, 7630−7634.

(31) Ostadhossein, A.; Rahnamoun, A.; Wang, Y.; Zhao, P.; Zhang, S.; Crespi, V. H.; van Duin, A. C. T. *J. Phys. Chem. Lett.* **2017**, *8*, 631−640.

(32) Castro-Marcano, F.; Kamat, A. M.; Russo, M. F.; van Duin, A. C. T.; Mathews, J. P. *Combust. Flame* **2012**, *159*, 1272−1285.

(33) Senftle, T. P.; Hong, S.; Islam, M. M.; Kylasa, S. B.; Zheng, Y.; Shin, Y. K.; Junkermeier, C.; Engel-Herbert, R.; Janik, M. J.; Aktulga, H. M.; Verstraelen, T.; Grama, A.; van Duin, A. C. T. *npj Comput. Mater.* **2016**, *2*, 15011.

(34) Akimov, A. V.; Prezhdo, O. V. *Chem. Rev.* **2015**, *115*, 5797−5890.

(35) Nosé, S. *J. Chem. Phys.* **1984**, *81*, 511−519.

(36) Hoover, W. G. *Phys. Rev. A: At., Mol., Opt. Phys.* **1985**, *31*, 1695.

(37) Taheri, P.; Wang, J.; Xing, H.; Destino, J. F.; Arik, M. M.; Zhao, C.; Kang, K.; Blizzard, B.; Zhang, L.; Zhao, P. *Mater. Res. Express* **2016**, *3*, 075009.

(38) Chen, C.; Feng, Z.; Feng, Y.; Yue, Y.; Qin, C.; Zhang, D.; Feng, W. *ACS Appl. Mater. Interfaces* **2016**, *8*, 19004−19011.

(39) Chen, J.; Tang, W.; Tian, B.; Liu, B.; Zhao, X.; Liu, Y.; Ren, T.; Liu, W.; Geng, D.; Jeong, H. Y. *Adv. Sci.* **2016**, *3*, 1500033.

(40) Liu, K.-K.; Zhang, W.; Lee, Y.-H.; Lin, Y.-C.; Chang, M.-T.; Su, C.-Y.; Chang, C.-S.; Li, H.; Shi, Y.; Zhang, H. *Nano Lett.* **2012**, *12*, 1538−1544.

(41) Liu, H.; Antwi, K. A.; Ying, J.; Chua, S.; Chi, D. *Nanotechnology* **2014**, *25*, 405702.

(42) Saburi, T.; Murata, H.; Suzuki, T.; Fujii, Y.; Kiuchi, K. *Purazuma·Kaku Yugo Gakkaishi* **2002**, *78*, 3−4.

DOI: 10.1021/acs.nanolett.7b01727
Nano Lett. 2017, 17, 4866−4872

(43) Weber, T.; Muijsers, J.; Van Wolput, J.; Verhagen, C.; Niemantsverdriet, J. *J. Phys. Chem.* **1996**, *100*, 14144−14150.
(44) Li, X. L.; Li, Y. D. *Chem. - Eur. J.* **2003**, *9*, 2726−2731.

DOI: 10.1021/acs.nanolett.7b01727
Nano Lett. 2017, 17, 4866−4872